The challenge in realizing an exchange coupled $BiFeO_3$ - double perovskite bilayer

Sven Becker[a,1], Sven Heinz[a,b], Mehran Vafaee[a], Mathias Kläui[a,b,c], Gerhard Jakob[a,b]

[a] *Institute of Physics, University of Mainz, Staudingerweg 7, 55128 Mainz*
[b] *Graduate School of Excellence Materials Science in Mainz (MAINZ), Staudingerweg 9, 55128 Mainz*
[c] *Center for Quantum Spintronics, Norwegian University of Science and Technology, Trondheim, Norway*

Abstract

In this work we propose a device design for efficient voltage control of magnetism. The magnetization of a ferrimagnetic double perovskite may be manipulated by an exchange coupled layer of multiferroic $BiFeO_3$. Bilayers of Barium doped $BiFeO_3$ and ferrimagnetic double perovskite Sr_2FeMoO_6 have been prepared by pulsed laser deposition motivated by the possibility of strong interlayer exchange coupling. While single layers of each material show high quality we observe that in both stacking orders the first layer decomposes during the deposition of the second layer. The reason for the decomposition are strongly differing growth conditions for $BiFeO_3$ and Sr_2FeMoO_6. This means that the generation of artificial multiferroic stacks requires careful choice of the constituent materials to ensure the bilayer stability.

Keywords: BiFeO3, Perovskite, Double Perovskite, Sr2FeMoO6, Exchange Bias, Exchange coupling

1. Introduction

One approach to realize a new generation of data storage device is to use an array of magnetic tunnel junction (MTJ) as bits. To efficiently manipulate the

[1] svenbecker@uni-mainz.de

state of the MTJ, one ferromagnetic (FM) layer is exchange coupled to a multiferroic (MF) antiferromagnet (AF). It has been shown that the magnetization manipulation of CoFe deposited on $BiFeO_3$ (BFO) is possible upon application of voltage at the BFO layer [1]. However, due to oxidization of the CoFe layer at the BFO interface the realization of a reliable device was not possible. Moving to an oxide FM layer the coupling to BFO was previously only observed up to a temperature of around 50 K [2]. We propose to use a ferrimagnetic electrode on top of the MF layer to achieve large coupling strength. Heteroepitaxy

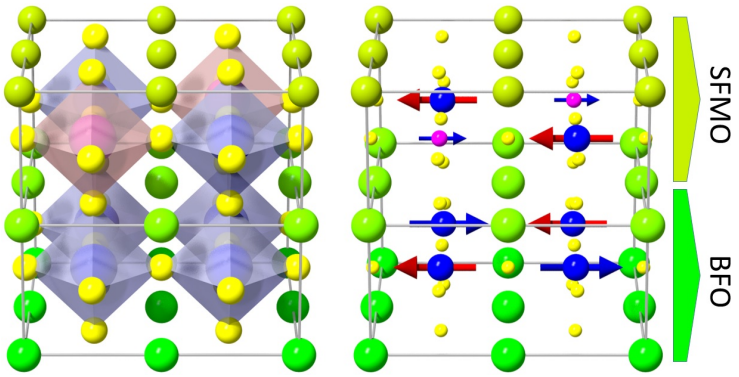

Figure 1: Crystal structures of BFO (bottom) and SFMO (top) demonstrating the structural (left) and magnetic (right) similarity. Spin directions and ionic sizes are not to scale.

offers the unique opportunity to have a perfect matching of spins of different layers. Perovskite heteroepitaxial multilayers have been fabricated in numerous publications. When combining the multiferroic BFO with the ferrimagnetic perovskite Sr_2FeMoO_6 (SFMO), we expect exchange coupling via the Fe - O - Mo and Fe - O - Fe bonds connecting the oxygen octahedra in the different layers. This is depicted in figure 1. All right pointing spins from Fe^{3+} of the G-type antiferromagnet BFO are expected to show an antiferromagnetic superexchange coupling to the Fe^{3+} ions of the SFMO. The left pointing spins from Fe^{3+} of BFO have only the negligible magnetic moment at the Mo^{5+} ions as superexchange partner. This leaves us with the overall magnetization being strongly coupled to the Néel vector of the BFO. In such a bilayer structure the rotation

of the BFO Néel vector by 180° may lead to the reversal of the SFMO magnetization due to the strong interlayer coupling. The antiferromagnetic interlayer coupling has already been observed in other magnetic oxide multilayers [3]. We choose the double perovskite Sr_2FeMoO_6 (SFMO) as conducting ferrimagnetic material because of it's high Curie temperature ($T_c > 410\,\mathrm{K}$ [4]) and a good lattice matching to $SrTiO_3$ (STO) substrate ($a = 3.905\,\text{Å}$). The lattice constants of bulk SFMO are $a = b = 5.568\,\text{Å}$ and $c = 7.897\,\text{Å}$ [5]. There is an in-plane lattice mismatch of 0.8% comparing the pseudocubic lattice constants (STO: $2a = 7.81\,\text{Å}$, SFMO: $a_{pc} = a \cdot \sqrt{2} = 7.87$). We choose Barium doped $BiFeO_3$ (BBFO) as MF layer. BBFO profits of less impurity phases than pure BFO and reduction of leakage current in polycrystalline bulk samples [6]. The lattice constant of bulk BBFO around is 3.98 Å and the symmetry of the unit cell changes from $R3c$ (pure BFO) to cubic [6]. The resulting lattice mismatch to STO is +1.9%. The exchange bias of a BFO/SFMO/STO stack system has been reported in [7]. Here we want to see if the exchange bias field can be increased by the choice of BBFO and the in-situ deposition of both layers. We also investigate the influence of the stacking order of the two layers.

2. Methods

Ba substituted $BiFeO_3$ samples with a Ba content of 15%, which corresponds to $Bi_{0.85}Ba_{0.15}FeO_3$ (BBFO), have been prepared by pulsed laser deposition from a target with 20% Bismuth excess to compensate loss during deposition [8, 9]. SFMO samples have been deposited from a stoichiometric target. The deposition chamber has a base pressure of $4 \cdot 10^{-8}$ mbar. The laser aperture of a Compex Pro 205 KrF excimer laser is projected on a $0.1\,\mathrm{cm}^2$ area creating a homogeneous energy distribution of around $640\,\mathrm{mJ/cm}^2$. As substrates, commercially available (001) oriented $SrTiO_3$ (STO) single crystals have been used after standard buffered HF treatment [10]. The substrate to target distance was fixed at 5.5 cm. Further growth conditions optimized for the respective materials are summarized in table 1. The samples have been analyzed concern-

Material	BBFO	SFMO
Background gas	O_2	Ar
Background pressure	0.1 mbar	0.1 mbar
Substrate temperature	475°C	750°C
Growth rate	1.0 Å/s	1.8 Å/s
Annealing	-	800°C
		1 h
		$1.4 \cdot 10^{-5}$ mbar O_2

Table 1: Deposition parameters for BBFO and SFMO single layers on STO substrates

ing their structural properties by X-ray diffraction in a *Bruker D8* four circle diffractometer. X-ray diffraction patterns were also simulated using CADEM software package [11]. The thickness of each sample is determined by X-ray reflectivity. Magnetic properties have been investigated using a *Quantum Design* SQUID magnetometer. For atomic force microscopy (AFM) as well as piezoresponse force microscopy (PFM) a *Digital Instruments 3100 Dimensions* equipped with a *NanoScope IV controller* has been utilized. In AFM mode the topology of the samples has been measured using *Bruker SNL-10* probes. In PFM mode ferroelectric domains have been manipulated and measured using *Bruker SCM-PIT* probes. To further analyze the topography of the samples a scanning electron microscope, a *FEI Helios NanoLab 600i*, was used. It is equipped with a dispersive X-ray spectrometer (EDX) to allow the measurement of the sample composition. For these measurements an operating voltage of 20 kV and a current of 5.5 nA was selected. The probing depth of the EDX is around 1 μm. Since we analyze only thin films of a few nanometer thickness no quantitative interpretation of the data is allowed but for qualitative comparison of different areas of the same sample it is suited.

3. Results and discussion

The $2\Theta/\omega$ scan of a BBFO(35 nm)/STO sample is shown in figure 2 a). We zoom in the range of interest around the (001) film and substrate peak since in the accessible range no other than the (00n) peaks of STO and BBFO are visible and to make the Laue oscillations of the film peak visible. From the film peak position we calculate an out-of-plane lattice constant of 4.2 Å. Reciprocal space maps around the (103) STO substrate peak (not shown) indicate that BBFO grows fully strained box-on-box on STO in a tetragonal phase with a $c : a$ ratio of 1.07 which coincides with the results from Mix et al. [9] for pure $BiFeO_3$ (BFO) on STO. In red is a CADEM simulation [11] of a XRD measurement of a sample

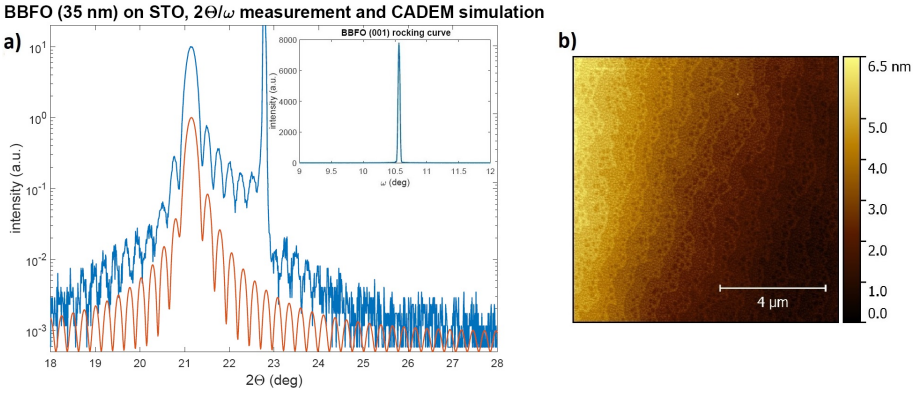

Figure 2: a) blue: $2\Theta/\omega$ scan of a 35 nm BBFO/STO sample grown at the conditions given in table 1. The left peak corresponds to the BBFO (001) reflex, the right peak to the (001) STO reflex. In red is a simulation of a XRD measurement at 84 unit cells of BBFO [11]. The curves are shifted for better visibility. The inset shows the rocking curve of the (001) BBFO peak. b) AFM scan of a BBFO/STO sample of similar thickness.

of 84 unit cells of BBFO with the corresponding out-of-plane lattice parameter. The simulation agrees well with the calculated data. The measured asymmetry of the first order Laue satellites can be well reproduced in the simulations with a gradual strain relaxation away from the interface with a decay length of 7 nm. The absence of other peaks and the occurrence of Laue oscillations indicate that BBFO grows smooth and single-phase. Omega scans of the (001) BBFO

reflex (inset) reveal a narrow rocking curve of $\omega = 0.03°$ FWHM indicating well oriented unit cells. The crystallinity of the BBFO samples is better than of the BFO samples that have been grown in our group before [2]. In addition, the surface roughness is very low as seen in figure 2 b). From the AFM image one can see that BBFO grows in a step-flow-like growth so that the steps of the STO substrate are reproduced by the thin film. The RMS roughness is below 1 nm. Also other groups report a reduction of impurity phases in the BFO single crystals when doping with Ba [12]. These advantages led us to use BBFO over BFO to achieve a smooth interface towards the SFMO. To show that the Ba substitution does not affect the ferroelectric properties of BFO the ferroelectric domain structure has been probed using piezoresponse force microscopy (PFM). For this purpose a stack of $SrRuO_3$ (SRO) bottom layer (20 nm) and BBFO top layer (50 nm) has been grown on STO substrate. Figure 3 shows the topography image as well as the phase- and amplitude image after applying +10 V between the AFM probe and the SRO bottom electrode while scanning a 1 μm square and -10 V in a 0.5 μm square (procedure known as PFM lithography). The frequency of the applied voltage during the succeeding PFM scan was kept constant at 356 kHz close to the contact resonance frequency. We observe no significant changes in the surface topography, but a prominent change in the phase- and amplitude measurement in the area of applied voltage. This indicates the switching of ferroelectric domains. The reversible manipulation of the FE domains indicate ferroelectric properties of BBFO.

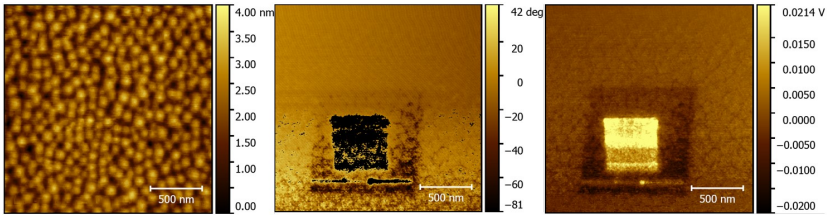

Figure 3: Measurement of topography (left), PFM phase (middle) and PFM amplitude (right) at the same time after PFM lithography at a sample BBFO (50 nm)/SRO (20 nm)/STO.

A $2\Theta/\omega$ scan of a SFMO(61 nm)/STO sample is shown in figure 4. No

other peaks than the film- and substrate reflexes are visible over a large scan range. The film peak is split into a double peak which indicates that SFMO grows partly in a strained and partly in a relaxed phase. Since there is a clear separation of the two peaks we assume that the we have a strained phase of the SFMO and a relaxed phase. The transition from strained to relaxed phase happens abruptly. A double Gaussian has been fitted to the double peak. The corresponding lattice constants are $c_S = 8.04$ and $c_R = 7.95$ Å. The bulk value given in literature is $c = 7.89$ Å. We calculate the lattice parameter according to Poisson's ratio under the assumption of heteroepitaxial strain to understand the lattice parameters. In case of perfect heteroepitaxy the in-plane lattice constants shrink to fit the substrate lattice and the out-of-plane lattice constant increases according to Poisson's ratio. In literature we find a Poisson's ratio for SFMO of $\nu = 0.36$ [13]. With this we calculate an expected lattice parameter of $c = 8.067$ Å. This value deviates from c_S by 0.3%. This deviation may stem from the in-plane lattice parameter of SFMO not exactly matching the STO or from off-stoichiometry. In figure 5 (a) we show a simulation of the XRD pattern using CADEM software [11]. We have a good agreement with the experimental data when we simulate 23 unit cells of strained and 25 unit cells of relaxed SFMO, corresponding to 18.5 nm and 19.9 nm, respectively. This is in good agreement with the experiment if we apply the Scherrer formula to the individual peaks (22 nm for strained, 18 nm for relaxed), which lends one to the conclusion that the assumption of two distinct phases is valid. As there exist additional effects leading to peak broadening the values calculated above are lower bounds for the actual size of the coherently scattering volume. Figure 5 (b) shows an atomic force microscopy (AFM) picture of the surface of the same SFMO sample indicating island-like growth. SFMO grows under epitaxial strain close to the surface. On top we expect relaxed SFMO that builds up to islands.

For the aim of growing a strongly exchange coupled bilayer it is essential to have large domains of SFMO with a well ordered B-site sublattice. We measure the B-site ordering of our sample by XRD. The intensity of the (111) reflex of

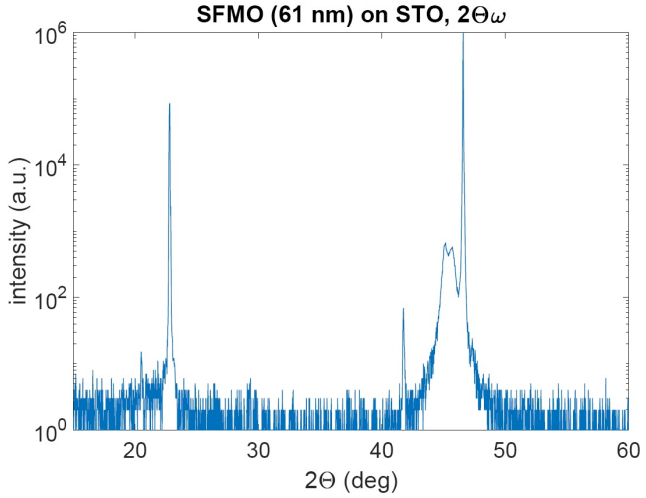

Figure 4: $2\Theta/\omega$ scan of a 61 nm SFMO/STO sample grown at the conditions given in table 1. The double peak on the left corresponds to SFMO (004) reflexes, the right peak to the (002) STO reflex. The SFMO is grown in two phases, a strained and a relaxed one.

SFMO depends on the B-site order of the material, in contrast to the (022) reflex, which is independent of the B-site ordering. The expected relative intensity of the (111) reflex for a perfectly ordered sample is $I_{(022)}/I_{(111)} = 26.25$. For completely disordered samples, this ratio would approach infinity. These relative intensity values are calculated with the help of PowderCell software, which simulates X-ray diffraction spectra for powder samples. The program is configured to use Bragg-Brentano geometry correction. For crystalline samples, we have to take into account the multiplicity of the individual peaks. For powder samples there are eight possibilities to have a crystallite oriented in the (111) direction and 12 possibilities for a grain oriented in the (022) direction. Since for crystalline samples we only see one crystal orientation at a time, we divide the relative peak intensity by the corresponding multiplicity to calculate the ratio for crystallite samples. We calculate a ratio of $I_{(022)}/I_{(111)} = 17.50$ for an ideal crystal. We take the area under the rocking curve as a measure for the relative peak intensity and determine a ratio of 28.67 for this sample. We achieve a similar value if we introduce a B-site disorder of 11% in our simulation.

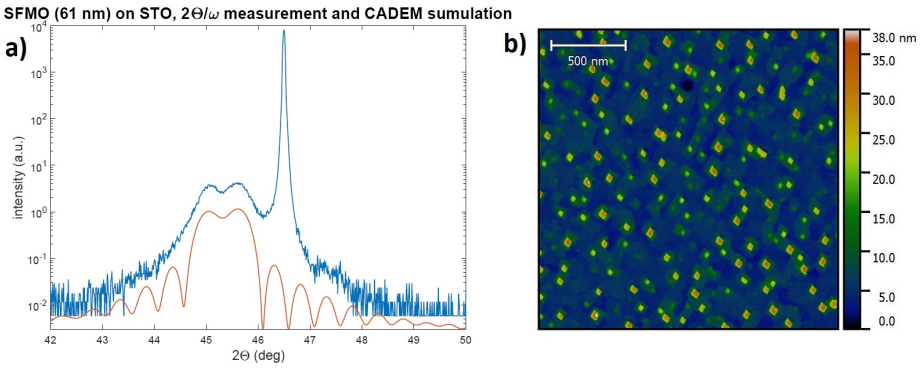

Figure 5: (a) Zoom of the $2\Theta/\omega$ scan around the (002) SFMO reflex (blue). In red the CADEM simulation of a sample of incoherent layers with two distinct lattice parameters. The curves are shifted for better visibility. (b) AFM picture of the same 61 nm SFMO/STO sample as in figure 5. To make islands as well as the morphology of the areas in between visible we choose a multicolor scaling.

A sample grown at the same conditions has been measured in a SQUID magnetometer. The Curie temperature has been determined by heating the sample in an applied field of 50 mT (39.79 kA/m). By linear interpolation we find a Curie temperature of around 360 K. The saturation magnetization has been determined at a temperature of 5 K. The hysteresis loop is shown in figure 6. After subtracting the diamagnetic contribution of the STO substrate we calculate a saturation magnetization of 2.8 μB/f.u. (212 kA/m), which differs from the theoretical value of 4 μB/f.u. [14] (303 kA/m). The coercivity is as large as 41 mT (3.87 kA/m)). In literature, we find similar values for the saturation magnetization and B-site disorder [15]. Sanchez-Soria [16] created samples with a saturation magnetization of around 3 μB/f.u. (227 kA/m) after extensive growth optimization.

Bilayers of SFMO and BBFO have been deposited in both possible stacking orders on STO substrates. The thickness of each SFMO layer is supposed to be 18 nm, the one of each BBFO layer is around 45 nm. We choose thin SFMO to increase the fraction of the strained phase and to increase the exchange bias field ($H_E \propto \frac{1}{t_{SFMO}}$). Large range $2\Theta/\omega$ scans of BBFO/SFMO/STO (BSS) and

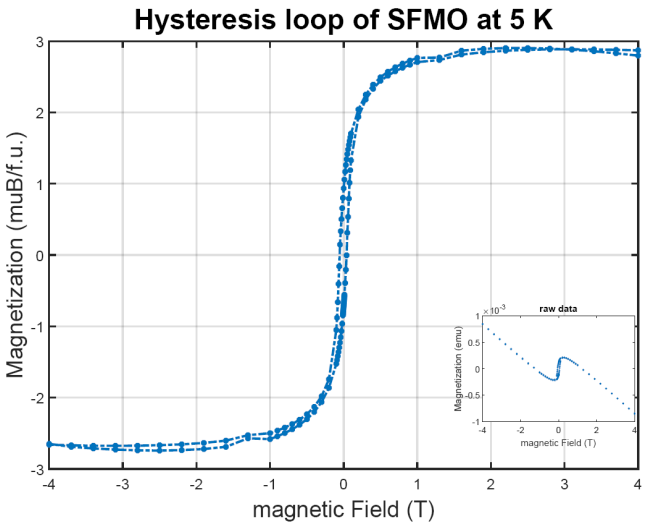

Figure 6: Hysteresis at a SFMO sample measured at 5 K. The saturation magnetization is 2.8 μB/f.u (212 kA/m), the coercive field is 41 mT (3.87 kA/m)).

SFMO/BBFO/STO (SBS) are shown in figure 7 a) and b).

In the BSS XRD scan one sees a broad peak to the left of both the (001) and (002) STO substrate peak. We do not observe the high crystalline quality of the BBFO layer as found for the BBFO/STO samples shown above (figure 2). There is no separation of the film reflexes. Therefore the determination of B-site disorder for the SFMO cannot be performed. Additional peaks around $2\Theta = 30°$ can be observed, indicating foreign phases. An absolute determination of these foreign phases from XRD only is not possible. We simulate an XRD measurement for $SrMoO_4$ (SMO) with the data from [17] since SMO is the most common impurity phase in SFMO. The peak with largest intensity of SMO is the (112), which should occur at $2\Theta = 29.4°$ for our measurement setup. The impurity peaks of the BSS sample are found at $2\Theta = 28.0°, 31.7°$ and 32.5°. Actually, we do not expect an exact matching since the stoichiometry of the impurity SMO may be $SrMoO_{4-\delta}$, altering the lattice parameter. Presence of SMO and Fe_xO_y phases in PLD-grown SFMO samples have already been reported [16, 18, 19]. The ex-situ decomposition at atmospheric conditions

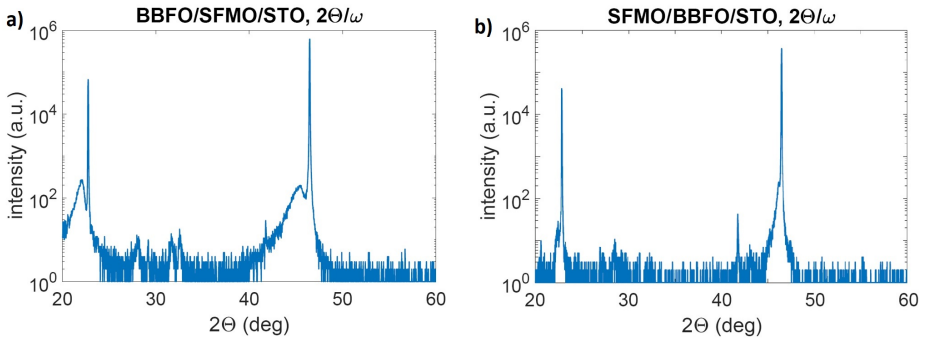

Figure 7: Large angle $2\Theta/\omega$ scan of a BFO/SFMO/STO sample (BSS) (a) and a SFMO/BFO/STO sample (SBS) (b), each including the (001) and (002) substrate peak.

is shown in [20]. The oxygen background pressure along with the high temperature during the BBFO deposition accelerate the aging process of the SFMO. So even in a foreign phase free layer strange phases grow inside the layer after the growth. In the SQUID magnetometer we observe the decreasing of saturation magnetization of SFMO down to 1.59 μB/f.u. (120 kA/m). This reduction

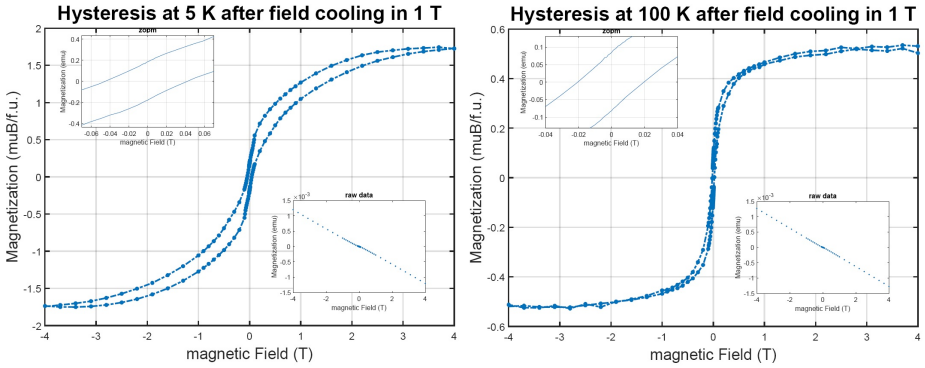

Figure 8: EB field measured by field cooling experiment. 1 T was applied while cooling from 390 K to 5 K (left) and 100 K (right), respectively.

compared to the single layer value may be attributed to the decomposition of the SFMO film. We measure an exchange bias field (H_{EB}) after cooling the sample under an applied field of 1 T as a measure for the interlayer coupling strength [2]. At 5 K we measure $H_{EB} = 1.8$ mT (3 kA/m). This is lower than

than reported values for BFO/LSMO [2] and BFO/SFMO [7]. At 100 K we calculate $H_{EB} = 0.6\,\mathrm{mT}$ (1 kA/m). The formation of SMO decreases the saturation magnetization of the layer and may lead to defects at the SFMO/BBFO interface. Because of the decomposition of the SFMO layer we do achieve the multiferroic/antiferromagnetic interface that we aim for. We do not end up with tetragonal distorted BBFO layer like reported in [7] for BFO/SFMO bilayers. A possible explanation is that BBFO is deposited at higher oxygen partial pressure. The further decomposition of the SFMO layer compared to the samples reported in [7] leads in comparison to a lower exchange bias field. Also the ex-situ hydrogen annealing, that was performed in [7] may have an impact on the stability of the SFMO layer.

To avoid the decomposition of SFMO the contact with oxygen needs to be prevented. A capping layer is no opportunity since we aim for a interlayer exchange coupling. The other solution is depositing the BBFO layer at very low oxygen partial pressure. However, we observe a strong reduction of the BBFO crystallographic quality when deposited at lower oxygen background pressure. In a second sample the order of layers are reversed so that BBFO is deposited first. In these samples of SBS stack order we do not see a peak at the (001) and (002) BBFO and SFMO peak positions. We observe a small signal at the shoulder of the STO substrate peak. The peak position at the (002) STO peak is 46.2°. Looking at the sample by eye, we observe an inhomogeneous material distribution. This lends itself to the interpretation that at the high deposition temperature of SFMO the previously deposited BBFO melted up into islands destroying the high quality BBFO layer. A scanning electron microscopy image is shown in figure 9. It shows such an island with magnification of 200x. In larger magnification one observes an increased roughness in the area of the island. We utilized EDX to compare the stoichiometry of the two different areas of the sample. This measurement is not suited for quantitative analysis of the sample because of it's thickness of only a few tens of nanometers compared to the information depth of around $1\,\mu$m of the measurement setup. A qualitative analysis is still allowed when comparing the results of the different areas of

the sample. The result is that the inhomogeneities do not stem from substrate contamination since no other elements but the deposited ones are observed. At the border of the island we observe a drastic change in the Fe:Bi ratio. The island seems to be Bi deficient and Fe rich, which indicates not only the melting but a phase separation of the BBFO layer. We conclude that the structure of the BBFO layer is completely destroyed and we do not perform measurements for determining the exchange bias field.

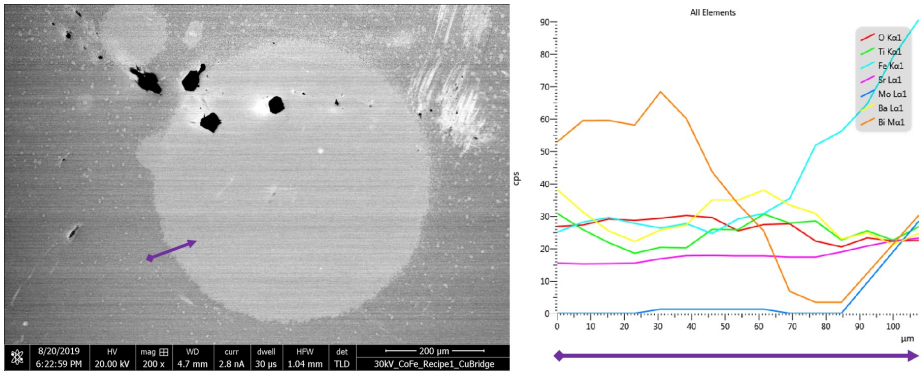

Figure 9: Microscopic image of a SBS sample surface taken by SEM. Black spots are carbon contaminations. The big circle is visible by eye and might be an island consisting of decomposed and molten BBFO. The arrow indicates the EDX scan area. The right image shows the EDX measurement at 15 measurement points along the arrow.

To avoid the decomposition of the BBFO layer one would need to protect it against high temperature. This can only be achieved by the deposition of the second layer at lower temperatures. Also the low oxygen pressure at elevated temperatures leads to the decomposition of BFO and the occurrence of BiO_x secondary phases [21]. This is also expected for BBFO. For SFMO, on the other hand, it is not possible to grow it under low temperature and elevated oxygen pressure. We conclude that the SBS stacking order is difficult to realized with the presented materials. For the BSS stacking order it has been shown that a bilayer grown with pure BFO is possible [7]. In the cited work the SFMO layer is ex-situ annealed after being deposited first and the pure BFO layer is grown at lower oxygen background pressure. For BBFO the high oxygen partial pressure

during the deposition seems to make the bilayer fabrication more difficult.

Since BFO has the unique property of being a single crystal room temperature multiferroic material with magnetoelectric coupling it seems to be harder to replace than the double perovskite at first sight. There exist over 720 different double perovskites with the generalized formula $A_2BB'O_6$ and a divalent A-site cation [22]. We want to evaluate the possibility of finding a ferrimagnetic perovskite that can be grown at lower temperature and higher oxygen pressure that SFMO. To find this material it is crucial to understand where the instability of the SFMO originates. In a simple picture Iron builds a Fe^{3+} ion forcing Molybdenum to create Mo^{5+} ion to generate a charge neutral unit cell. However, Mo^{5+} is a rather unusual oxidation state, since Mo^{6+} is more stable. This can be seen by the existence of Molybdenum oxides. Other than MoO_3 the existence of Mo_2O_5 is not reported. This shows that indeed the 5+ oxidation state is very unlikely. Therefore the probability for the creation of a SMO strange phase is very high at elevated oxygen background pressure due to the formation of Mo^{6+} ions. However, the origin of the ferrimagnetic coupling in SFMO is the double exchange interaction between Fe and Mo, originating in the near degeneracy of the two valence states $Fe^{3+}-Mo^{5+}$ and $Fe^{2+}-Mo^{6+}$ in the double perovskite structure [23, 24]. So one may check if there are elements that have both 5+ and 6+ stable oxidation states. Among the $4d$ and $5d$ elements there is actually no element fulfilling this condition. There seems to be a tradeoff between ferrimagnetic coupling and stability of the double perovskite. The most studied conducting ferrimagnetic double perovskites with T_C over room temperature besides SFMO are Sr_2FeReO_6, Sr_2CrWO_6 [15]. Both materials seem to suffer from the same instability mechanism like SFMO. A clear indicator is that Sr_2CrWO_6 thin films are deposited in pure Argon atmosphere [25] and for Sr_2FeReO_6, of which thin films have not been prepared to our knowledge, powder samples build foreign phases of $Sr_5Re_2O_{12}$ at the grain surfaces [26]. Going to Sr_2CrReO_6 [27] or Sr_2CrOsO_6 [28] the double perovskite become insulating while keeping it's ferrimagnetic ordering above room temperature. In these compounds the hybridization effect becomes weak and superexchange coupling has to be taken

into account. The growth of Sr_2CrReO_6 is done by PLD under a low oxygen partial pressure of around $3.6 \cdot 10^{-5}$ mbar and Sr_2CrOsO_6 polycrystalline samples are heated under an oxygen flow after fabrication. This may indicate that the stability against oxidation is higher compared to the hybridization-based perovskites. Moving to an insulating ferrimagnet our device concept presented in the introduction would need to be modified. So far we have only discussed the influence of the B- and B'-cation, but also the A-site cation has an influence on the properties of the double perovskite that might be taken into account. Not only that the geometric stability of the unit cell is influenced (Goldschmidt tolerance factor), but also the valence of the B- and B'-ion [29]. Summarizing one can say that although the number of double perovskites is huge, the number of those suited for the presented device concept is limited. Conducting ferrimagnets seem to be lacking of stability against oxidation while insulating ones are not useful for the application we aimed for. One may combine the best properties of both kinds of compounds by doping. This field still requires research especially concerning the stability of the compounds. The postulated half-metallicity of doped Sr_2CrOsO_6 [30] gives hope in finding a suited material for voltage controlled magnetic tunneling junctions.

4. Conclusion

We determined the conditions for optimal deposition of BBFO and SFMO layers. Both BBFO and SFMO single layers deposited on $SrTiO_3$ (STO) substrates show high crystalline quality. BBFO layers have smooth surfaces and exhibit ferroelectric properties in piezoresponse force microscopy measurements. SFMO grows fully epitaxial on STO up to a thickness of around 20 to 25 nm. The B-site disorder is calculated from the intensity of X-ray reflexes. We achieve a disorder as low as around 11%. We point out the challenge in the realization of such a material stack due to the different growth conditions. Depositing SFMO as a first layer in pure argon background pressure, the layer decomposes due to the formation of a $SrMoO_4$ phase during the deposition of BBFO in

pure oxygen atmosphere, which results in a poor interlayer coupling. When depositing BBFO as a first layer we observe melting of the BBFO layer at the high deposition temperature of SFMO. We conclude that the particular material combination is not well suited for bilayer fabrication. To achieve exchange coupled bilayers one has to take into account the stability of each layer.

5. Acknowledgements

The authors gratefully acknowledge funding by the Deutsche Forschungsgemeinschaft (DFG, German Research Foundation) - project numbers 358671374 and 121583221 as well the Graduate School of Excellence Material Science in Mainz (GSC266). This work was supported by the Max Planck Graduate Center with the Johannes Gutenberg-Universitt Mainz (MPGC). Funded by the Deutsche Forschungsgemeinschaft (DFG, German Research Foundation) - TRR 173 - 268565370.

References

[1] J. T. Heron, J. L. Bosse, Q. He, Y. Gao, M. Trassin, L. Ye, J. D. Clarkson, C. Wang, J. Liu, S. Salahuddin, D. C. Ralph, D. G. Schlom, J. Íñiguez, B. D. Huey, R. Ramesh, Deterministic switching of ferromagnetism at room temperature using an electric field, Nature 516 (2014) 370–373. doi:10.1038/nature14004.

[2] M. Vafaee, S. Finizio, H. Deniz, D. Hesse, H. Zabel, G. Jakob, M. Kläui, The effect of interface roughness on exchange bias in $La_{0.7}Sr_{0.3}MnO_3-BiFeO_3$ heterostructures, Applied Physics Letters 108 (7) (2016) 072401. doi:10.1063/1.4941795.

[3] S. Das, A. D. Rata, I. V. Maznichenko, S. Agrestini, E. Pippel, N. Gauquelin, J. Verbeeck, K. Chen, S. M. Valvidares, H. Babu Vasili, J. Herrero-Martin, E. Pellegrin, K. Nenkov, A. Herklotz, A. Ernst, I. Mertig, Z. Hu, K. Dörr, Low-field switching of noncollinear spin texture

at $La_{0.7}Sr_{0.3}MnO_3$−$SrRuO_3$ interfaces, Phys. Rev. B 99 (2019) 024416. doi:10.1103/PhysRevB.99.024416.

[4] Y. Tomioka, T. Okuda, Y. Okimoto, R. Kumai, K.-I. Kobayashi, Y. Tokura, Magnetic and electronic properties of a single crystal of ordered double perovskite Sr_2FeMoO_6, Physical Review B 61 (2000) 422–427. doi:10.1103/PhysRevB.61.422.

[5] K.-I. Kobayashi, T. Kimura, H. Sawada, K. Terakura, Y. Tokura, Room-temperature magnetoresistance in an oxide material with an ordered double-perovskite structure, Nature 395 (6703) (1998) 677–680. doi:10.1038/27167.

[6] A. Makhdoom, M. Akhtar, M. Rafiq, M. Hassan, Investigation of transport behavior in Ba doped $BiFeO_3$, Ceramics International 38 (5) (2012) 3829 – 3834. doi:https://doi.org/10.1016/j.ceramint.2012.01.032.

[7] C. Chen, L. Guo, C. Li, B. Gao, R. Zheng, J. Wang, Q. Li, J. Du, Q. Xu, Exchange bias in tetragonal-like $BiFeO_3/Sr_2FeMoO_6$ bilayer, Journal of Magnetism and Magnetic Materials 464 (2018) 156 – 160. doi:https://doi.org/10.1016/j.jmmm.2018.05.063.

[8] H. Béa, M. Bibes, A. Barthélémy, K. Bouzehouane, E. Jacquet, A. Khodan, J.-P. Contour, S. Fusil, F. Wyczisk, A. Forget, D. Lebeugle, D. Colson, M. Viret, Influence of parasitic phases on the properties of $BiFeO_3$ epitaxial thin films, Applied Physics Letters 87 (7) (2005) 072508. doi:10.1063/1.2009808.

[9] C. Mix, G. Jakob, Multiferroic and structural properties of $BiFeO_3$ close to the strain induced phase transition on different substrates, Journal of Applied Physics 113 (17) (2013) 17D907. doi:10.1063/1.4795216.

[10] G. Koster, B. L. Kropman, G. J. H. M. Rijnders, D. H. A. Blank, H. Rogalla, Quasi-ideal strontium titanate crystal surfaces through formation of

strontium hydroxide, Applied Physics Letters 73 (20) (1998) 2920–2922. doi:10.1063/1.122630.

[11] P. Komar, G. Jakob, *CADEM*: calculate X-ray diffraction of epitaxial multilayers, Journal of Applied Crystallography 50 (1) (2017) 288–292. doi:10.1107/S1600576716018379.

[12] R. Das, K. Mandal, Magnetic, ferroelectric and magnetoelectric properties of Ba-doped $BiFeO_3$, Journal of Magnetism and Magnetic Materials 324 (11) (2012) 1913 – 1918. doi:https://doi.org/10.1016/j.jmmm.2012.01.022.

[13] R. Lu, H. Wu, Y. Qian, E. Kan, Y. Liu, W. Tan, C. Xiao, K. Deng, The effect of biaxial mechanical strain on the physical properties of double perovskite Sr_2FeMoO_6: A theoretical study, Solid State Communications 191 (2014) 70 – 75. doi:https://doi.org/10.1016/j.ssc.2014.03.017.

[14] A. S. Ogale, S. B. Ogale, R. Ramesh, T. Venkatesan, Octahedral cation site disorder effects on magnetization in double-perovskite Sr_2FeMoO_6: Monte carlo simulation study, Applied Physics Letters 75 (4) (1999) 537–539. doi:10.1063/1.124440.

[15] D. Serrate, J. M. D. Teresa, M. R. Ibarra, Double perovskites with ferromagnetism above room temperature, Journal of Physics: Condensed Matter 19 (2) (2006) 023201. doi:10.1088/0953-8984/19/2/023201.

[16] D. Sánchez, M. García-Hernández, N. Auth, G. Jakob, Structural, magnetic, and transport properties of high-quality epitaxial Sr_2FeMoO_6 thin films prepared by pulsed laser deposition, Journal of Applied Physics 96 (5) (2004) 2736–2742. doi:10.1063/1.1774244.

[17] E. Gürmen, E. Daniels, J. S. King, Crystal structure refinement of $SrMoO_4$, $SrWO_4$, $CaMoO_4$, and $BaWO_4$ by neutron diffraction, The Journal of Chemical Physics 55 (3) (1971) 1093–1097. doi:10.1063/1.1676191.

[18] H. Deniz, D. Preziosi, M. Alexe, D. Hesse, C. Eisenschmidt, G. Schmidt, L. Pintilie, Microstructure and properties of epitaxial Sr_2FeMoO_6 films containing $SrMoO_4$ precipitates, Journal of Materials Science 50 (8) (2015) 3131–3138. doi:10.1007/s10853-015-8874-7.

[19] I. Angervo, M. Saloaro, J. Tikkanen, H. Huhtinen, P. Paturi, Improving the surface structure of high quality Sr_2FeMoO_6 thin films for multilayer structures, Applied Surface Science 396 (2017) 754 – 759. doi:10.1016/j.apsusc.2016.11.021.

[20] J. Navarro, C. Frontera, D. Rubi, N. Mestres, J. Fontcuberta, Aging of Sr_2FeMoO_6 and related oxides, Materials Research Bulletin 38 (9) (2003) 1477 – 1486. doi:10.1016/S0025-5408(03)00171-5.

[21] H. A. Begum, H. Naganuma, M. Oogane, Y. Ando, Fabrication of multiferroic Co-substituted $BiFeO_3$ epitaxial films on $SrTiO_3$ (100) substrates by radio frequency magnetron sputtering, Materials 4 (6) (2011) 1087–1095. doi:10.3390/ma4061087.

[22] S. Vasala, M. Karppinen, A_2BBO_6 perovskites: A review, Progress in Solid State Chemistry 43 (1) (2015) 1 – 36. doi:https://doi.org/10.1016/j.progsolidstchem.2014.08.001.

[23] J.-S. Kang, J. H. Kim, A. Sekiyama, S. Kasai, S. Suga, S. W. Han, K. H. Kim, T. Muro, Y. Saitoh, C. Hwang, C. G. Olson, B. J. Park, B. W. Lee, J. H. Shim, J. H. Park, B. I. Min, Bulk-sensitive photoemission spectroscopy of A_2FeMoO_6 double perovskites ($A = \mathrm{Sr}, \mathrm{Ba}$), Phys. Rev. B 66 (2002) 113105. doi:10.1103/PhysRevB.66.113105.

[24] J. Lindén, T. Yamamoto, M. Karppinen, H. Yamauchi, T. Pietari, Evidence for valence fluctuation of Fe in Sr_2FeMoO_{6-w} double perovskite, Applied Physics Letters 76 (20) (2000) 2925–2927. doi:10.1063/1.126518.

[25] J. B. Philipp, D. Reisinger, M. Schonecke, M. Opel, A. Marx, A. Erb, L. Alff, R. Gross, Epitaxial growth and transport properties of Sr_2CrWO_6

thin films, Journal of Applied Physics 93 (10) (2003) 6853–6855. doi:10.1063/1.1556124.

[26] M. Retuerto, F. Jimnez-Villacorta, M. J. Martínez-Lope, Y. Huttel, E. Roman, M. T. Fernández-Díaz, J. A. Alonso, Study of the valence state and electronic structure in Sr_2FeMO_6 (M = W, Mo, Re and Sb) double perovskites, Phys. Chem. Chem. Phys. 12 (2010) 13616–13625. doi:10.1039/C004370B.

[27] A. J. Hauser, J. R. Soliz, M. Dixit, R. E. A. Williams, M. A. Susner, B. Peters, L. M. Mier, T. L. Gustafson, M. D. Sumption, H. L. Fraser, P. M. Woodward, F. Y. Yang, Fully ordered Sr_2CrReO_6 epitaxial films: A high-temperature ferrimagnetic semiconductor, Phys. Rev. B 85 (2012) 161201. doi:10.1103/PhysRevB.85.161201.

[28] Y. Krockenberger, K. Mogare, M. Reehuis, M. Tovar, M. Jansen, G. Vaitheeswaran, V. Kanchana, F. Bultmark, A. Delin, F. Wilhelm, A. Rogalev, A. Winkler, L. Alff, Sr_2CrOsO_6: End point of a spin-polarized metal-insulator transition by $5d$ band filling, Phys. Rev. B 75 (2007) 020404. doi:10.1103/PhysRevB.75.020404.

[29] Y. Yasukawa, J. Lindn, T. Chan, R. Liu, H. Yamauchi, M. Karppinen, Iron valence in double-perovskite $(Ba,Sr,Ca)_2FeMoO_6$: isovalent substitution effect, Journal of Solid State Chemistry 177 (8) (2004) 2655 – 2662. doi:https://doi.org/10.1016/j.jssc.2004.04.031.

[30] K. Samanta, P. Sanyal, T. Saha-Dasgupta, Half-metallic behavior in doped Sr_2CrOsO_6 double perovskite with high transition temperature, Scientific Reports 5 (1). doi:10.1038/srep15010.